JOURNAL OF NANO- AND ELECTRONIC PHYSICS
Vol. 18 No 3, 03027(5pp) (2026)

ЖУРНАЛ НАНО- ТА ЕЛЕКТРОННОЇ ФІЗИКИ
Том 18 № 3, 03027(5cc) (2026)

REGULAR ARTICLE

Design and Optimization of a Plant-Structured MIMO Antenna for Advanced Wireless Wi-Fi 6E Systems

Francis Mulagani[1], K. Vasu Babu[2,*], Sudipta Das[3], Praveen Mallik[1], Anusha Rani Medarametla[1]

[1] *School of Electronics and Electrical Engineering, Lovely Professional University, Phagwara, Punjab, India*
[2] *Department of ECE, BVRIT Hyderabad College of Engineering for Women, Telangana, India*
[3] *Department of ECE, IMPS College of Engineering and Technology, West Bengal, India*

(Received 10 March 2026; revised manuscript received 20 June 2026; published online 26 June 2026)

This study introduces a compact plant-structured MIMO antenna developed for modern wireless applications, including Wi-Fi 6E and IoT Systems. The design structure is implemented on substrate of FR-4 with a small footprint as 45 mm × 20 mm, which makes it well suited for miniaturized wireless devices. The antenna resonates at 6.98 GHz with IBW of 1.8 GHz (5.5-7.3 GHz) effectively covering the upper C-band band for Wi-Fi 6E and IoT Systems. The achieved simulated S_{11} result of − 19.33 dB verifies good matching of impedance characteristics. The mutual coupling within MIMO elements is limited to − 19.89 dB (S_{21}) demonstrating efficient isolation performance. An inter-element spacing of 6.5 mm is preserved to further minimize electromagnetic interaction. Important MIMO performance indicators such as Total Active type Reflection Coefficient (TARC), Channel type Capacity Loss (CCL), Diversity related Gain (DG) and Envelope Correlation type Coefficient (ECC) are comprehensively analyzed. All evaluated MIMO parameters remain within the standard acceptable limits confirming dependable wireless system operation. The obtained results reveal excellent diversity behavior, minimal correlation and enhanced channel capacity. Therefore, designed plant-structured MIMO system serves as a strong for compact, efficient and reliable for Wi-Fi 6E and IoT Systems.

Keywords: Antenna, Wi-Fi 6E and IoT systems, Return loss, Channel capacity loss, Mutual coupling, MIMO system.

DOI: 10.21272/jnep.18(3).03027 PACS number: 84.40.Ba

1. INTRODUCTION

Antenna play a vital role in wireless communication systems. In recent times, to fulfil the requirements of high data rates and improved network capacity of modern advanced wireless systems, MIMO antennas are on high demands. Researchers have reported many MIMO designs in literature, such as a flower-inspired broadband radiator [1] for sub-6 GHz 5G systems is developed using CMA, while a dual-band MIMO configuration optimized for radar sensing is reported in [2]. A low-profile ultra-wideband MIMO antenna with three notch bands is introduced in [3], and a four-element MIMO structure for IR-UWB applications exhibits efficient dual-notch suppression and multitone interference rejection [4]. A dual-stopband slotted-edge substrate antenna is proposed in [5]. Further advancements include a DGS-assisted MIMO antenna with a feature of interference reduction [6], and a CPW-excited MIMO antenna supporting dual-notch characteristics and GSM operation [7]. A Wang-shaped geometry [8] is shown to significantly minimize inter-element coupling. The use of Gaussian process techniques for radiator optimization is discussed in [9], while a compact radiator employing parasitic elements with machine-learning-based optimization is presented in [10] for sub-6 GHz 5G platforms. Moreover, a slot-loaded inverted-F MIMO antenna, reported in [11] enable WLAN dual-band functionality, followed by a semi-circular compact dual-band arrangement, discussed in [12]. A small-sized four-port DGS-based radiator with integrated notch filtering is described in [13], and a printed 4-element MIMO system optimized for ISM band is reported [14]. A CSRR-embedded compact four-port radiator [15] achieves wideband operation with high isolation, whereas a compact dual-band printed MIMO system [16] covers X-band, WLAN, sub-6 GHz, and WiMAX bands. Deep-learning-driven surrogate models for antenna synthesis are proposed in [17] to improve precision and reduce design time. An 8-element MIMO dual-band array suitable for 5G handheld components is demonstrated in [18].

Although numerous studies on MIMO antennas have been carried out in literature, still there is growing demands for MIMO antenna with novel design techniques to support advanced applications such as Wi-Fi 6E and IoT Systems. In this article, a MIMO antenna having plant-like geometry is designed, which resonates at 6.98 GHz covering 5.5 GHz to 7.3 GHz broad spectrum, with excellent resonance, radiation and diversity metrics. Compact size, good impedance matching, novel geometry, broad operating bandwidth, and superior MIMO diversity features are the prime novelties of this article.

* Correspondence e-mail: vasubabuece@gmail.com

Cite this article as: F. Mulagani et al., *J. Nano- Electron. Phys.* 18 No 3, 03027 (2026) https://doi.org/10.21272/jnep.18(3).03027

2. ANTENNA LAYOUT AND ARCHITECTURE

Fig. 1(a) illustrates the top view geometry of a two-element MIMO antenna printed on a rectangular dielectric substrate. The red region represents the substrate, while the olive-colored patterns correspond to the metallic radiating elements and feed structures. The overall dimensions of the antenna are defined by *W* (width) and *L* (length). Each antenna element consists of a compact snowflake/star-shaped radiator formed by multiple arms (labeled *p*, *q*, *r*, *s*, *t*, *u*, etc.), which increase the effective electrical length and enable resonance at the desired operating frequency within a compact physical size. The narrow vertical strip at the center of each radiator acts as the feed line that excites the antenna element. The parameters *x*, *y*, *j*, and other marked lengths indicate critical geometrical dimensions that control impedance matching, resonant frequency, and bandwidth. The separation *x* denotes the center-to-center spacing between two-antenna elements and plays a key role in mutual coupling reduction and improving MIMO performance.

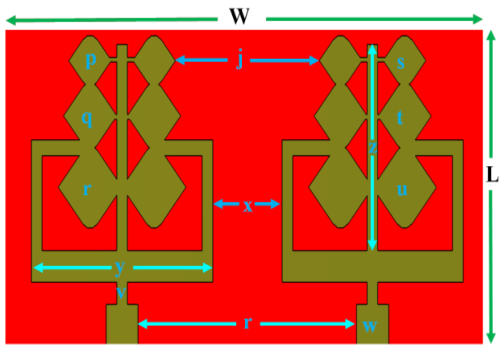

(a)

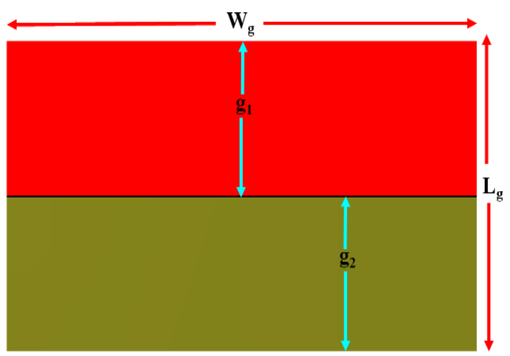

(b)

Fig. 1 – Plant structured design (a) Upper view (b) Lower view

The bottom feed sections with width w represent the input ports for Port-1 and Port-2 excitation. Overall, the symmetric placement of the two radiators and careful optimization of spacing and arm dimensions ensure good isolation, compact size, and stable radiation characteristics suitable for MIMO wireless applications. Fig. 1 (b) represents the backside (ground plane) configuration of designed structure. The total width and length of ground plane are denoted by W_g and L_g. The ground plane is divided into two sections such as the upper red portion and the lower olive portion, indicating a partial or defected ground structure (DGS). The parameter g_1 corresponds to the height of the upper ground segment, while g_2 represents the height of the lower ground segment. This segmentation of the ground plane is intentionally introduced to modify distribution of surface current and the effective capacitance and inductance of antenna system. By properly choosing g_1 and g_2, the impedance matching, bandwidth, and isolation between MIMO elements can be significantly improved. Such a partial ground plane structure enhances radiation efficiency and helps in achieving better control over radiator resonant characteristics which is making it especially useful for MIMO radiator designs where reduction in mutual coupling and wideband performance is critical.

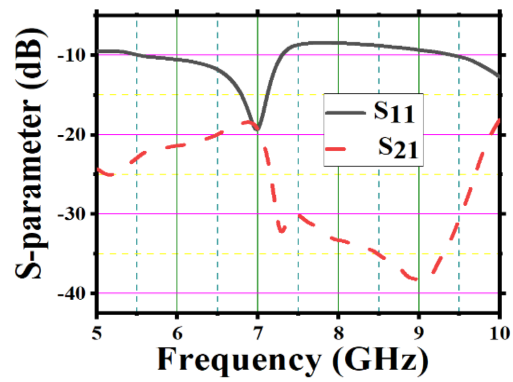

(a)

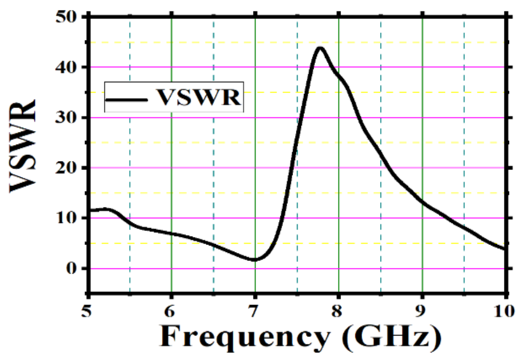

(b)

Fig. 2 – Plant MIMO structured design (a) S-parameters (b) VSWR

Fig. 2(a) shows *S*-parameters of simulated designed MIMO system over frequency range 5-10 GHz. The solid black curve represents S_{11} which indicates the input S_{11} and hence matching of impedance. A clear resonance is observed around 6.98 GHz, here S_{11} goes below – 20 dB, confirming good efficient radiation and impedance matching at this operating region. Throughout most of the band, S_{11} is below – 10 dB, indicating acceptable matching performance. The red dashed curve corresponds to S_{21}, which represents the mutual coupling among elements of radaitor. The values of S_{21} remain well below – 20 dB across a wide portion of the band and reach minima close to – 35 dB near frequency of resonance. This demonstrates strong isolation within MIMO system and effective suppression of inter-element interference. Fig. 2(b) illustrates variation of the VSWR related to proposed radiator over 5-10 GHz range. VSWR is an important parameter that indicates quality of matching of impedance between radiator and the feeding line of transmission. A lower VSWR signifies efficient matching and more efficient power transfer. From the plot, VSWR crosses minimum value around 6.98 GHz, where it is reaches to 1 which confirming excellent matching of impedance at the resonant frequency. In this region, the radaitor operates most efficiently with the minimal reflected power. As the frequency moves away from resonance, the VSWR increases, indicating a gradual mismatch. A sharp rise in VSWR is observed around 8 GHz, which corresponds to a stopband behavior, possibly due to structural resonance or the presence of notching characteristics.

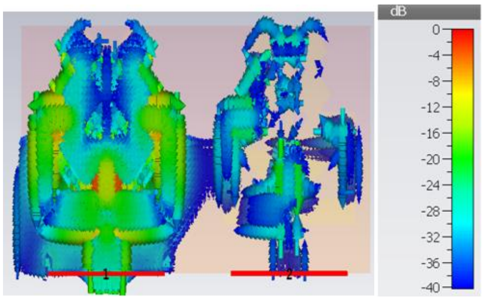

(a)

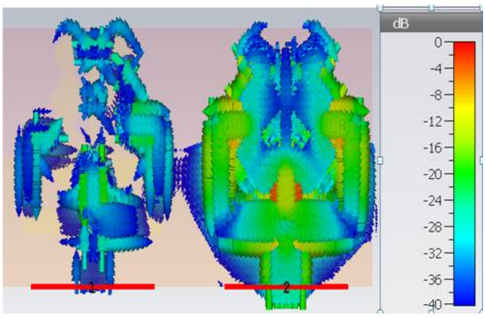

(b)

Fig. 3 – Surface current distributions at 6.98 GHz when (a) Port 1 excited (b) Port 2 excited

Fig. 3(a) shows distribution of surface currents related to 2-element MIMO radiator when 1st port is excited and other port is ended with matched load. The color bar in dB indicates magnitude related to surface current, where red and yellow indicate strong current concentration, while green and blue correspond to moderate and weak current levels, respectively. From the plot, one can observe that a high current density is majorly confined to excited antenna element, particularly along the feeding line and the edges of the radiator, confirming effective excitation and radiation. The non-excited element exhibits very weak current levels, mostly shown in blue, which indicates minimal induced currents. This behavior demonstrates strong isolation between the two MIMO elements and effective suppression of mutual coupling. Additionally, the distribution of currents along the arms of the radiator highlights their role in increasing the electrical path length and supporting resonance at the desired operating frequency. The limited current leakage toward the adjacent element validates the efficiency of the antenna geometry and spacing strategy in achieving good MIMO performance. Overall, this figure confirms that the proposed design provides strong confinement of surface currents, reduced inter-element interaction, and enhanced isolation characteristics. Similarly, Fig. 3(b) depicts distribution of surface current of two-element MIMO radaitor when excitation is applied to the second port, while first port is ended with matched load. The color scale in dB represents the current intensity, where red and yellow indicate strong surface currents, and green to blue indicate progressively weaker currents.It is clearly observed that the right-side antenna element (excited port) exhibits a strong concentration of surface current, particularly around the feed line and along the arms of the radiator. This confirms efficient excitation and proper radiation from the active element. In contrast, the left-side element shows very low current levels, mainly in blue shades, indicating that only negligible induced currents are present. This behavior verifies excellent isolation between the two antenna elements, as very little electromagnetic energy is coupled from the excited radiator to the adjacent one. The symmetric nature of the current distribution compared to the previous case (when Port-1 was excited) also demonstrates that both antenna elements operate equivalently and independently. Table 1 shows structural dimensions of the plant design are measured in mm. The radiation patterns of the proposed MIMO antenna for both *E*- and *H*-fields are plotted in Fig. 4, fulfilling the requirements for intended applications.

Table 1 – All structural dimensions of plant structure are in mm

W	L	p	q	r	s	W_g	L_g
45	20	4	4	4	4	45	20
g_1	t	u	g_2	v	x	j	y
10	4	4	10	2	6.5	12	8

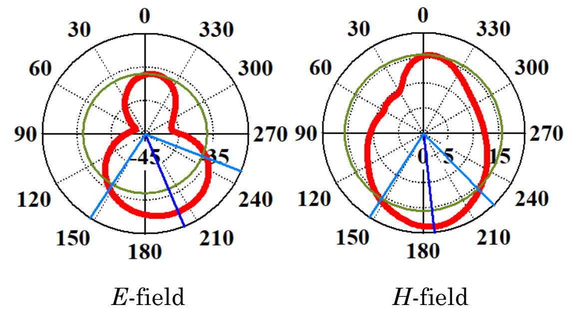

Fig. 4 – Radiation characteristics of the proposed MIMO antenna

3. MIMO METRICS INVESTIGATION

Various MIMO diversity metrics are utilized to assess performance related to MIMO system under the conditions of multipath propagation. The ECC evaluates extent of decoupling among antenna ports in wireless communication systems, where a smaller ECC value indicates superior port isolation and enhanced diversity characteristics of the designed MIMO radiator. In this study, the ECC is calculated using equation (1) to verify for effectiveness of designed configuration and obtained results remain within acceptable limits throughout the operating frequency bands, confirming optimal antenna behavior.

An additional ECC evaluation technique is also implemented using equation (2). Fig. 5(a) presents the simulated ECC characteristics. For effective diversity operation in MIMO systems, ECC value below 0.05 [18] and simulated ECC of the proposed antenna is observed to be ≤ 0.0109, which clearly meets this criterion and validates its practical applicability. Moreover, DG is a crucial metric which improves the signal-to-noise ratio in communication regions employing diversity schemes and is typically expressed in decibels (dB). Fig. 5 (b) illustrates the frequency response of diversity gain, exhibiting values close to 9.9999 dB around the resonant frequency region. The computation of DG from ECC is performed using equation (3) as reported in [9], which further verifies the outstanding related to diversity MIMO system.

$$ECC_{i,j} = \frac{\left|\iint_{4\pi}\left[\vec{E_i}(\theta,\phi).\vec{E_j}(\theta,\phi)d\Omega\right]\right|^2}{\iint_{4\pi}\left|\vec{E_i}(\theta,\phi)\right|^2 d\Omega \iint_{4\pi}\left|\vec{E_j}(\theta,\phi)\right|^2 d\Omega} \quad (1)$$

$$ECC_{i,j} = \frac{\left|S_{ii}^{*}S_{ij}+S_{ji}^{*}S_{jj}\right|^2}{\left(1-|S_{ii}|^2-|S_{ji}|^2\right)\left(1-|S_{jj}|^2-|S_{ij}|^2\right)} \quad (2)$$

$$\mathrm{DG}_{i,j}=10\sqrt{1\text{-}\left|\mathrm{ECC}_{i,j}\right|^2} \quad (3)$$

The TARC is another significant parameter in MIMO systems, defined as square-root ratio of power to total incident power and reflected power. It considers the influence of random phase excitations at all ports while simultaneously accounting for coupling within antenna elements. TARC is essential for evaluating the radiation efficiency and impedance bandwidth performance of MIMO antennas under various excitation conditions. In this work, TARC is calculated using the expression given in equation (4) [12]. Fig. 5 (c) shows the frequency response of TARC, where the values are below − 10 dB around band of resonant which indicating satisfactory radiation characteristics of proposed MIMO configuration.

$$TARC = \frac{\sqrt{\sum_{i=1}^{N}\left|S_{lm}+S_{lm}e^{j\theta_{m-1}}\right|}}{\sqrt{N}} \quad (4)$$

CCL is another key diversity metric used to analyze the performance of MIMO antennas, as it reflects maximum achievable reduction data transmission rate caused by correlation and coupling effects. It represents the limitation in complete signal transfer across the communication channel due to frequency-dependent losses. For efficient MIMO operation, the acceptable CCL value should be less than 0.15 bps/Hz [8]. The mathematical expressions used to compute CCL are provided in equations (5)-(7). The evaluated CCL results are depicted in Fig. 5(d), remaining below 0.25 bps/Hz over all resonant frequency ranges.

$$C_{loss} = -\log_2 det(\Psi^R) \quad (5)$$

$$\rho_{ii} = 1-\left(\sum_{j=1}^{8}\left|S_{ij}\right|^2\right) \quad (6)$$

$$\rho_{i,j} = -\left(S_{ii}^{*}S_{ij}+S_{ji}^{*}S_{jj}\right) \quad (7)$$

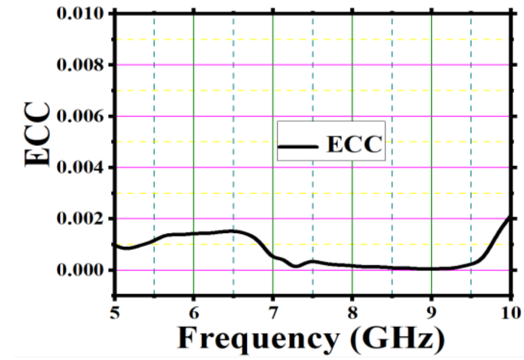

(a)

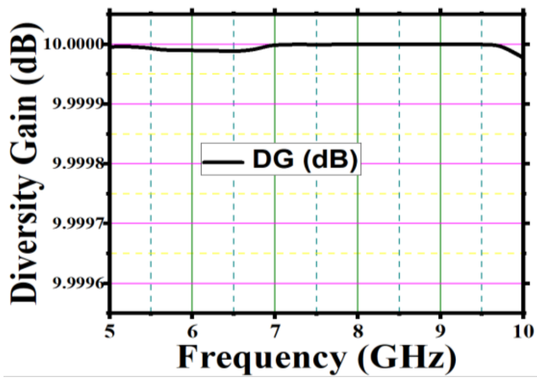

(b)

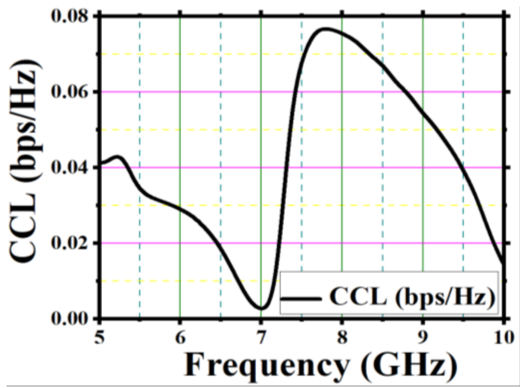

(c)

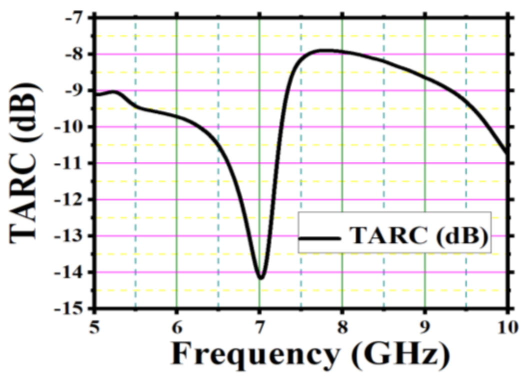

(d)

Fig. 5 – MIMO parameter (a) ECC (b) DG (c) TARC (d) CCL

4. CONCLUSION

In conclusion, a compact plant-structured MIMO antenna related to Wi-Fi 6E and IoT systems has been successfully designed and analyzed. The radaitor is fabricated on substrate related as FR-4 with 45 mm × 20 mm, making it highly appropriate for miniaturized wireless devices. The proposed structure exhibits stable resonance at 6.98 GHz, effectively covering the upper C-band required for Wi-Fi 6E and IoT systems. The achieved reflection coefficient of − 19.33 dB confirms good impedance matching, while the measured mutual coupling of − 19.89 dB (S_{21}) demonstrates strong isolation between the MIMO elements. An optimized inter-element spacing of 6.5 mm further contributes to the reduction of electromagnetic interaction. Moreover, key MIMO performance metrics, including TARC, CCL, DG, and ECC, have been thoroughly evaluated and found to remain within standard acceptable limits. These results validate excellent diversity performance, low signal correlation, and improved channel capacity. Overall, the proposed plant-structured MIMO antenna proves to be a compact, efficient, and reliable solution making a promising for next-generation Wi-Fi 6E & IoT wireless communication systems.

REFERENCES

1. K.V. Babu, S. Das, S.S. Ali, M. El. Ghzaoui, B.T.P. Madhav, S.K. Patel, *Int. J. Commun. Syst.* **36** No 6, e5442 (2023) https://doi.org/10.1002/dac.5442.
2. K.V. Babu, S. Kokkirigadda, S. Das, *Lecture Notes Elect. Eng.*, 792 (Springer: Singapore: 2022) https://doi.org/10.1007/978-981-16-4625-6_29
3. D.K. Raheja, B.K. Kanaujia, S. Kumar, *Int. J. RF Microwave Comput-Aid. Eng.* **29** No 10, e21831 (2019) https://doi.org/10.1002/mmce.21831.
4. M. Shehata, M.S. Said, H. Mostafa, *IEEE Trans. Antennas Propag.* **66** No 11, 5737 (2018) https://doi.org/10.1109/TAP.2018.2868725.
5. D.K. Raheja, B.K. Kanaujia, S. Kumar, *Int. J. RF Microwave Comput-Aid. Eng.* **27**, e21756 (2019) https://doi.org/10.1002/mmce.21756.
6. K.V. Babu, B. Anuradha, *Microwave Opt. Technol. Lett.* **61** No 12, 2698 (2019) https://doi.org/10.1002/mop.31958.
7. K. Srivastava, A. Kumar, B.K. Kanaujia, S. Dwari, S. Kumar, *Int. J. RF Microwave Comput.-Aid. Eng.* **29** No 1, e21433 (2019) https://doi.org/10.1002/mmce.21433.
8. K.V. Babu, B. Anuradha, *Analog Integr. Circ. Sig. Process.* **101** No 1, 67 (2019) https://doi.org/10.1007/s10470-019-01397-y.
9. X-Y. Zhang, Y-B. Tian, X. Zheng, *Int. J. Antennas Propag.* **2020**, 2154928 (2020) https://doi.org/10.1155/2020/2154928.
10. K.V. Babu, S. Das, G.N.J. Sree, S.K. Patel, M.P. Saradhi, M.R.N. Tagore, *AEU-Int. J. Electron. Commun.* **153**, 154281 (2022) https://doi.org/10.1016/j.aeue.2022.154281.
11. W-J. Liao, C-Y. Hsieh, B-Y. Dai, B-R, Hsiao, *IEEE Antennas Wireless Propag. Lett.* **14**, 847 (2014) https://doi.org/10.1109/LAWP.2014.2381362.
12. K.V. Babu, P.S. Rao, B.C. Naik, B.R. Kumar, *Microsyst. Technol.* **29**, 501 (2023) https://doi.org/10.1007/s00542-022-05359-9.
13. P. Pannu, Preeti, D.K. Sharma, *Int. J. RF Microwave Comput.-Aid. Eng.* **30** No 9, e22288 (2020) https://doi.org/10.1002/mmce.22288.
14. K. Kaboutari, V. Hosseini, *AEU-Int. J. Electron. Commun.* **134**, 153687 (2021) https://doi.org/10.1016/j.aeue.2021.153687.
15. A. Kumar, A.Q. Ansari, B.K. Kanaujia, J. Kishor, *Frequenz* **72** No 9-10, 415 (2018) https://doi.org/10.1515/freq-2017-0276.
16. K.V. Babu, S. Das, S. Lakrit, S.K. Patel, B.T.P. Madhav, H. Medkour, *Progress In Electromagnetics Research C* **117**, 99 (2021).
17. N. Koziel, Çalık, P. Mahouti, M.A. Belen, *IEEE Trans. Antennas Propag.* **71** No 1, 105 (2023) https://doi.org/10.1109/TAP.2022.3216064.
18. K. Yan, P. Yang, F. Yang, L.Y. Zeng, S. Huang, *2018 IEEE International Symposium on Antennas and Propagation & USNC/URSI National Radio Science Meeting*, 41 (Boston, MA: USA: 2018).

Проєктування та оптимізація MIMO-антени з рослинною структурою для передових бездротових систем Wi-Fi 6E

Francis Mulagani[1], K. Vasu Babu[2], Sudipta Das[3], Praveen Mallik[1], Anusha Rani Medarametla[1]

[1] *School of Electronics and Electrical Engineering, Lovely Professional University, Phagwara, Punjab, India*
[2] *Department of ECE, BVRIT Hyderabad College of Engineering for Women, Telangana, India*
[3] *Department of ECE, IMPS College of Engineering and Technology, West Bengal, India*

Представлено компактну MIMO-антену заводської конструкції, розроблену для сучасних бездротових застосувань, включаючи системи Wi-Fi 6E та IoT. Конструкція реалізована на підкладці з FR-4 з малими розмірами 45 мм × 20 мм, що робить її добре придатною для мініатюрних бездротових пристроїв. Антена резонує на частоті 6,98 ГГц з IBW 1,8 ГГц (5,5-7,3 ГГц), ефективно покриваючи верхній діапазон C для систем Wi-Fi 6E та IoT. Отриманий результат моделювання $S11$ – 19,33 дБ підтверджує хорошу відповідність характеристик імпедансу. Взаємний зв'язок всередині елементів MIMO обмежений до – 19,89 дБ ($S21$), що демонструє ефективну ізоляцію. Міжелементна відстань 6,5 мм зберігається для подальшої мінімізації електромагнітної взаємодії. Всебічно проаналізовано важливі показники продуктивності MIMO, такі як загальний коефіцієнт відбиття активного типу (TARC), втрати ємності каналу (CCL), коефіцієнт підсилення, пов'язаний з рознесенням (DG), та коефіцієнт кореляції обвідної (ECC). Усі оцінені параметри MIMO залишаються в межах стандартних допустимих значень, що підтверджує надійну роботу бездротової системи. Отримані результати демонструють чудову поведінку рознесення, мінімальну кореляцію та покращену пропускну здатність каналу. Таким чином, розроблена система MIMO з планово-обладнаною структурою слугує потужним засобом для компактного, ефективного та надійного використання в системах Wi-Fi 6E та Інтернету речей.

Ключові слова: Антена, Системи Wi-Fi 6E та IoT, Втрати на відбиття, Втрати пропускної здатності каналу, Взаємний зв'язок, Система MIMO.